

**Calculation of excited polaron states in the Holstein model**

O. S. Barišić\*

*Institute of Physics, Bijenička c. 46, HR-10000 Zagreb, Croatia*

(Received 10 November 2002; revised manuscript received 17 November 2003; published 12 February 2004)

An exact-diagonalization technique is used to investigate the low-lying excited polaron states in the Holstein model for the infinite one-dimensional lattice. For moderate values of the adiabatic ratio, a comprehensive picture, involving three excited (coherent) polaron bands below the phonon threshold, is obtained. The coherent contribution of the excited states to both the single-electron spectral density and the optical conductivity is evaluated and, due to the invariance of the Hamiltonian under the space inversion, the two are shown to contain complementary information about the single-electron system at zero temperature. The chosen method reveals the connection between the excited bands and the renormalized local phonon excitations of the adiabatic theory, as well as the regime of parameters for which the electron self-energy has notable nonlocal contributions. Finally, it is shown that the hybridization of two polaron states allows a simple description of the ground and first excited states in the crossover regime.

DOI: 10.1103/PhysRevB.69.064302

PACS number(s): 71.38.-k, 63.20.Kr

**I. INTRODUCTION**

Although more than half of a century has elapsed since Landau proposed that the charge carrier could be trapped by the distortion of a crystal lattice<sup>1</sup> and Pekar introduced the term polaron,<sup>2</sup> a number of questions regarding the single-polaron theory remain unanswered. This is true even in the context of the Holstein Hamiltonian,<sup>3</sup> one of the simplest electron-lattice coupling models for the one-electron system. While the literature pertaining to the ground state of such a model is extensive, much less attention has been paid to the excited states, even at the low energies for which they are most interesting.

The nature of the excited polaron states has been investigated within the adiabatic approximation in Refs. 4–6 by neglecting the polaron translation. These works provide a simple picture of the self-trapped polaron states for strong couplings. That is, the adiabatic softening of the phonon modes within the self-trapped polaron states results in several excitation energies below the bare phonon energy. It follows that the lowest excitations of the system are the polaron states for which the electron and phonons are strongly correlated. When the polaron translation is restored, each of the soft-phonon modes below the bare phonon energy can be expected to develop the corresponding band if the local dynamics remains adiabatic. Actually, moving polarons have been described within the adiabatic approximation by neglecting the force impeding the polaron translational motion due to the lattice discreteness.<sup>7–9</sup> However, the band structure of the spectrum was not considered in these investigations. For strong couplings, the bandwidth of the lowest band has been obtained by the adiabatic theory in the context of the simplest two-site model.<sup>10,11</sup>

When considering the band structure it is important to realize that the polaron states are coherent in the range of energies below the phonon threshold (i.e., below the minimal energy for inelastic scattering).<sup>12,13</sup> One way to investigate their properties is by analyzing the single-electron and optical conductivity spectra. In the case of the single-polaron problem, the low-frequency coherent part of the spectral

weight directly determines the polaron energies. Most of the previous spectral investigations,<sup>14–20</sup> however, make no mention of the excited coherent polaron bands. The exceptions in this respect are provided by those works employing the dynamic mean-field theory (DMFT), which is exact in the infinite-dimensional limit. The DMFT results predict one excited polaron band below the phonon threshold.<sup>13,21</sup>

For the one-dimensional system, recent exact-diagonalization (ED) and variational approaches<sup>22,23</sup> obtained results for the lowest state of the first excited band. Provided that the local electron dynamics remains adiabatic and that the adiabatic calculation of the self-trapped polaron energies gives several solutions below the inelastic phonon threshold, more than one excited polaron band is expected to occur in this energy range. The present paper shows that the ED approaches for the infinite lattice, as implemented in recent works,<sup>22–25</sup> can be extended to give very accurate results for the first few excited coherent polaron bands. In the range of parameters for which the method converges, the coherent part of the spectrum is found to exhibit up to three excited polaron bands, two more than previously described. These results provide a better understanding of the spatial and temporal structure of the polaron states, as well as of their symmetry (parity) properties. The latter can be used to rationalize the contributions of the bands to the low-energy single-electron and optical conductivity spectra, respectively.

An additional and attractive feature of the excitation spectrum obtained herein is its potential to help clarify the physical picture of the polaron crossover for moderate values of the adiabatic ratio. It has been previously proposed,<sup>23</sup> in the context of the variational analysis,<sup>23,26</sup> that this crossover, in which the ground state evolves from a light to a heavy polaron state, can be understood as the anticrossing (hybridization) of two low-energy states. This question is reconsidered here in terms of practically exact eigenstates and their aforementioned parity properties. Specifically, hybridization is found to occur between states of equal parity, whereas states of opposite parity cross without any such hybridization. Furthermore, the hybridization of states in the crossover regime is characteristic not only of the Holstein model under con-

sideration. Recently, for example, on the basis of accurate numerical results obtained by the diagrammatic quantum Monte Carlo method<sup>27</sup> for the Rashba-Pekar polaron model,<sup>28</sup> it has been suggested that the polaron crossover in that instance also involves a hybridization of several polaron solutions.<sup>29</sup>

ED methods, analogous to the one employed here, have found widespread application in the ground-state calculations of numerous other many-body problems. In this context, the present analysis of the excited states, together with their symmetry attributes, is also of interest for the description of low-energy eigenstates and spectral properties from a more general point of view.

## II. HOLSTEIN POLARON PROBLEM

The one-dimensional Holstein model of interest here is defined by the Hamiltonian

$$\hat{H} = -t \sum_n c_n^\dagger (c_{n+1} + c_{n-1}) + \hbar\omega \sum_n b_n^\dagger b_n - g \sum_n c_n^\dagger c_n (b_n^\dagger + b_n). \quad (1)$$

Here  $t$  is nearest-neighbor hopping energy of the electron and  $\hbar\omega$  is the energy of dispersionless optical phonons, while  $g$  is the electron-phonon coupling energy.  $c_n^\dagger$  and  $b_n^\dagger$  are creation operators for the electron and phonon at lattice site  $n$ , respectively. As only the single-electron problem is treated, the spin indices have been omitted.

The total momentum of the system ( $\hat{K}$ ) is the sum of electron and phonon momenta. As  $\hat{K}$  commutes with the Hamiltonian (1), the complete set of states of the system can be constructed from eigenstates of  $\hat{H}$  and  $\hat{K}$ . The Hamiltonian (1) is also invariant under space inversion. However, the analysis of the resulting parity properties of the eigenstates will be deferred until later in the present discussion (Sec. IV D).

The eigenstates that will be considered herein are those falling in the energy window defined by

$$E_{K=0}^{(0)} \leq E < E^{(c)}, \quad E^{(c)} = E_{K=0}^{(0)} + \hbar\omega. \quad (2)$$

$E_{K=0}^{(0)}$  is the minimal energy of the system (the zero-momentum polaron ground-state energy) and  $\hbar\omega$  is the energy of the bare phonon excitation. When the electron-phonon coupling is absent ( $g=0$ ) the states below the phonon threshold  $E^{(c)}$  are those of the free-electron band. When  $g$  is switched on, the free-electron states evolve into those states correlated with phonons. Furthermore, additional bands can appear below  $E^{(c)}$  as the coupling increases. All states in the energy window (2) are correlated and will be referred to as polaron states. For  $E \geq E^{(c)}$  the electron and additional phonons can form weakly bound states, which results in a highly degenerate spectrum.

The energies of the coherent polaron states are henceforth denoted by  $E_K^{(i)}$  and the wave functions by  $|\Psi_K^{(i)}\rangle$ .  $K$  is the momentum of the polaron state (which is also the system

momentum), while  $i$  denotes the band index. The lowest (ground) polaron band will be denoted by  $i=0$ . In the present paper the term ground state is used for the state of minimal energy for a given momentum  $K$  and not to the  $K=0$  state only. Accordingly, the first excited state corresponds to the first excited state of a given momentum  $K$  and so forth.

For the polaron bands below the phonon threshold  $E^{(c)}$  the states  $|\Psi_K^{(i)}\rangle$  are the eigenstates of  $b_{q=0}$  (Refs. 30 and 31):

$$b_{q=0} |\Psi_K^{(i)}\rangle = \frac{1}{\sqrt{N}} \sum_n b_n |\Psi_K^{(i)}\rangle = \frac{1}{\sqrt{N}} \frac{g}{\hbar\omega} |\Psi_K^{(i)}\rangle.$$

More generally, it can be shown that for all eigenstates  $|\Psi_K^E\rangle$  the simple sum rule for the mean total lattice deformation, given by

$$\bar{x}_{tot} = \sum_n \bar{x}_n = x_0 \sum_n \langle \Psi_K^E | (b_n^\dagger + b_n) | \Psi_K^E \rangle = \frac{2gx_0}{\hbar\omega}, \quad (3)$$

is satisfied. In Eq. (3),  $x_0$  is the space uncertainty of the free harmonic oscillator with frequency  $\omega$ . Besides its physical meaning, the sum rule for the mean total lattice deformation can also be used as a tool for checking the validity of results obtained with approximate polaron wave functions.

## III. EXACT-TRANSLATIONAL METHOD

In the case of the Holstein polaron problem, the ED approach uses only a finite number of states which contribute significantly to the exact polaron wave function for a given set of Hamiltonian parameters. By using the Hamiltonian matrix corresponding to the truncated (reduced) basis and the appropriate numerical scheme, one calculates the polaron wave functions and energies. The convergence of the results can be verified by increasing the number of basis states in the calculation. In most cases the results are very accurate, provided that the truncation procedure is well chosen.

The ED method developed in the current paper is henceforth referred to as the exact-translational method (ET method). The basis states of the ET method are given by<sup>22</sup>

$$|n_0, n_{-1}, n_1, \dots, n_m\rangle_K = \frac{1}{\sqrt{N}} \sum_j e^{iKja} c_j^\dagger |n_0, n_{-1}, n_1, \dots, n_m\rangle_j. \quad (4)$$

The orthonormal wave function (4) describes an electron which is surrounded by a cloud of phonons. The number of phonons at the  $m$ th lattice site away from the electron is given by  $n_m$ , while  $K$  corresponds to the total system momentum and  $a$  is the lattice constant. The basis states (4) of different momenta  $K$  are not mixed by the Holstein Hamiltonian.

If the adiabatic ratio  $t/\hbar\omega$  is not too large, the ET method can be used for studying polarons in the weak- and strong-coupling regimes, as well as in the crossover regime between them. The present paper is focused, particularly, on the regime in which  $1 \lesssim t/\hbar\omega \lesssim 5$  and  $g$  is arbitrary. For  $g, t$

$\gg \hbar\omega$ , the number of relevant basis states (4) becomes large and the problem of finding the polaron wave functions becomes untreatable. Unfortunately, the limit  $g, t \gg \hbar\omega$ , which is not considered here, is difficult for other known numerical methods as well.

The matrix representation of the Holstein Hamiltonian in the ET basis leads to a sparse matrix. That is, it is straightforward to show that, by acting on the state (4) with the Hamiltonian (1), the maximum number of nonzero matrix elements per ET basis state is 5. As an example, let us form the reduced Hilbert space of only five ET states—i.e., of the zero-phonon state  $|0\rangle_K$ , of three states with one phonon (phonon at the electron site, at the left site from the electron, and at the right site from the electron),

$$|n_0=1\rangle_K, |n_{-1}=1\rangle_K, |n_1=1\rangle_K,$$

and finally, of the state with two phonons at the electron site  $|n_0=2\rangle_K$ . The corresponding Hamiltonian matrix is given by

$$\begin{bmatrix} -2t \cos Ka & g & 0 & 0 & 0 \\ g & \hbar\omega & -te^{-iKa} & -te^{iKa} & g\sqrt{2} \\ 0 & -te^{iKa} & \hbar\omega & 0 & 0 \\ 0 & -te^{-iKa} & 0 & \hbar\omega & 0 \\ 0 & g\sqrt{2} & 0 & 0 & 2\hbar\omega \end{bmatrix}.$$

In the limit  $g, t \ll \hbar\omega$  the ET method gives a good polaron ground state with only these five states. Nevertheless, for  $t \sim \hbar\omega$  one usually has to work with a truncated basis of quite large dimension. In other words, the ET method generally requires a numerical scheme capable of dealing with large sparse matrices.

For this purpose the well-known Lanczos algorithm appears to be the most appropriate choice.<sup>32,33</sup> Indeed, previous papers using the ET method for ground-state calculations have employed this technique. An additional, attractive, feature of the Lanczos algorithm is that it is capable of finding not just one, but rather a few extreme eigenvalues (and eigenvectors) of sparse matrices, provided they are well separated (lying in the discrete part of the spectrum). Accordingly, the current results have been obtained by the Lanczos procedure with so-called local orthogonalization. In addition, the states have been calculated by the block-Lanczos procedure, with both variants giving the same results.

It should be stressed that the present results are compared to the already cited ground-state results<sup>22–24</sup> of the ET method. All states are checked through the sum rule (3), as well as through their mutual orthogonality.

#### IV. POLARON BANDS

##### A. Numerical results

At the beginning of our discussion it is instructive to observe how the polaron bands are formed in regard to the strength of the electron-phonon coupling  $g$ . For this purpose, the polaron bands are plotted in the four panels of Fig. 1 as functions of the momentum ( $K$ ), for  $t=5$  and different val-

ues of  $g$ . As in the remainder of the paper,  $\hbar\omega=1$  is used as the energy unit. Notice that, as discussed in connection with Eq. (2), only the part of the spectrum below the phonon threshold (between  $E_{K=0}^{(0)}$  and  $E^{(c)}$ ) is shown.

In the weak-coupling limit for the lowest band ( $i=0$ ), two regimes exist with respect to the critical momentum  $K_c$  (Refs. 34 and 35). For  $K \lesssim K_c$  the polaron state of energy  $E_K^{(0)} < E^{(c)}$  is the ground state of the system. For  $K \gtrsim K_c$  the ground state consists of the polaron and the unbound phonon excitation. The unbound phonon excitation carries the system momentum  $K$ , while the polaron momentum is equal to 0. For  $K \gtrsim K_c$  the ground-state energy lies at the bottom of the incoherent part of the spectrum  $E \geq E^{(c)}$ . The first panel of Fig. 1 shows the ET weak-coupling results. Notice that the top flat part of the lowest band for  $K \gtrsim K_c$  has been cut by the frame. The reason is that the numerical error of the corresponding ET states is slightly greater than that of the zero-momentum ground state, while the energy interval shown is exactly equal to the bare phonon energy  $\hbar\omega$ . As the electron-phonon coupling increases, the lowest band becomes more renormalized, and finally, at some critical coupling, the whole band falls below  $E^{(c)}$ .

By increasing electron-phonon coupling further, the additional polaron bands emerge below  $E^{(c)}$ . In the second and third panels of Fig. 1 the results for  $g=2.8$  and  $g=3.3$  are shown, respectively. These are the choices of parameters that correspond to the crossover regime. For  $g=2.8$ , only a part of the first excited band ( $i=1$ ) lies below  $E^{(c)}$ , whereas for  $g=3.3$  there are four polaron bands in the relevant energy window. From the third panel of Fig. 1 ( $g=3.3$ ) one sees that the top of the second excited band ( $i=2$ ) is at  $K=0$  and the bottom is at  $K=\pi/a$ . In addition, this band ( $i=2$ ) crosses the other excited bands ( $i=1,3$ )—i.e., the first excited band near the end of the Brillouin zone (for  $g \lesssim 3.3$ ) and the third excited band near the center of the Brillouin zone.

For strong couplings ( $g=3.85$ ) the ET results are shown in the last panel of Fig. 1. All the bands are very narrow. Although it is hard to distinguish the third excited band ( $i=3$ ) from the plot frame, note that  $E_K^{(3)} < E^{(c)}$  for all  $K$ .

Figure 2 gives further insight into the polaron band formation. Here, the  $K=0$  and  $K=\pi/a$  energy curves, shifted by  $E_{K=0}^{(0)}$ , are plotted for four bands ( $i$  is the band index). The results are presented for the crossover and strong-coupling regimes. In the weak-coupling regime (not shown in Fig. 2)  $E_{K=\pi/a}^{(0)}$  becomes smaller than  $E^{(c)}$  for  $g \approx 1.6$ .

It can be seen from Fig. 2 that the bandwidth of the lowest band decreases continuously with  $g$ . On the other hand, the bandwidth of the first excited state shows a more complicated behavior. Namely, for  $g \approx 3.15$  this bandwidth is maximal, while, unlike for the lowest band, it decreases for smaller values of  $g$ . Its maximal value and the minimum of  $E_{K=0}^{(1)} - E_{K=0}^{(0)}$  ( $g \approx 3.2$ ) correspond to similar electron-phonon couplings. From Fig. 2 the band crossing which involves the second and the two other excited bands can be clearly seen to occur in the crossover regime. That fact that these bands cross each other indicates that they belong to different symmetries, as will be discussed further below (Sec. IV D).

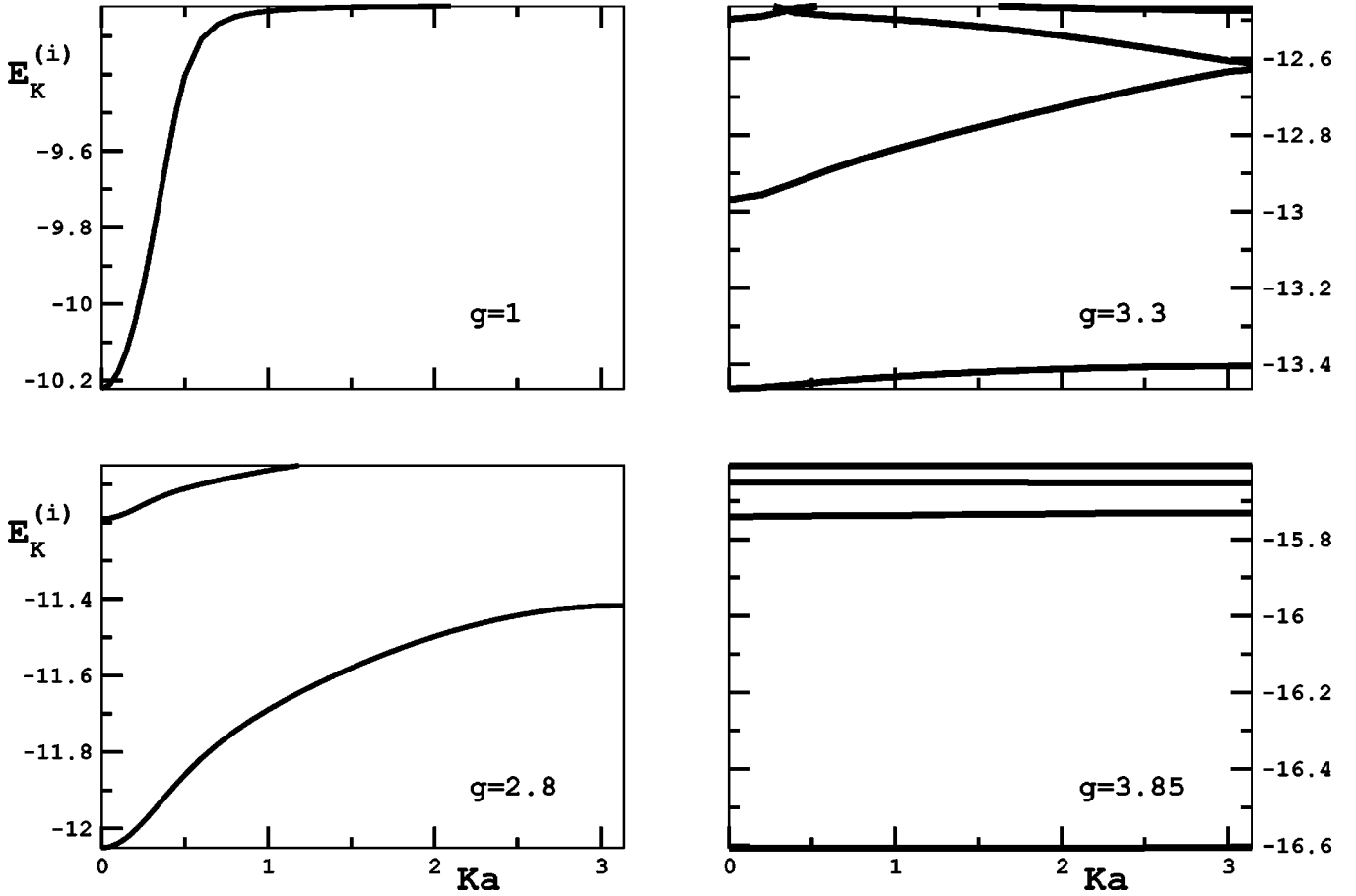


FIG. 1. The polaron bands are plotted as functions of momentum ( $K$ ) for  $t=5$  and four different values of  $g$ .  $\hbar\omega=1$  defines the energy unit used throughout this paper. The results for  $g=1$  and  $g=3.85$  correspond to the weak- and strong-coupling regimes, respectively, whereas results for  $g=2.8$  and  $g=3.3$  correspond to the crossover regime. Only the part of spectrum below the phonon threshold  $E \leq E^{(c)}$  is shown.

In the strong-coupling regime the spectrum consists of very narrow bands. Although in Fig. 2 the bands are well separated, for very large couplings all of the excited bands approach  $E^{(c)}$  from below. Finally, it can be seen from Fig. 2 that, for  $t=5$ , the energy of the third excited band stays close

to  $E^{(c)}$  in both the crossover and strong-coupling regimes. The  $K$  values corresponding to the top of the third excited band depend sensitively on the Hamiltonian parameters. It should therefore be kept in mind that, in contrast to the other bands, the  $K=\pi/a$  curve only approximately determines the boundary of this band. In particular, the third excited band is slightly wider than suggested by Fig. 2 in the crossover regime.

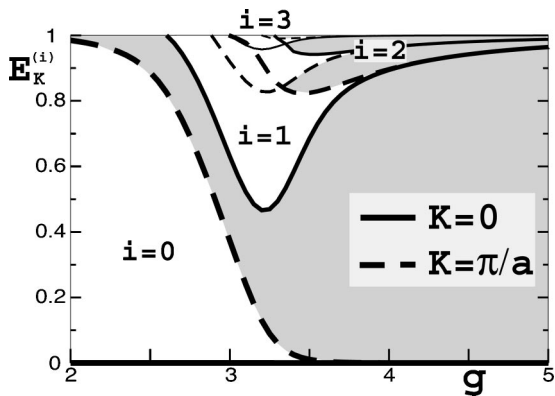


FIG. 2. The polaron bands below the phonon threshold shifted by  $E_{K=0}^{(0)}$  are plotted as functions of  $g$  for  $t=5$  ( $\hbar\omega=1$ ). The band boundaries correspond to  $E_{K=0}^{(i)}$  and  $E_{K=\pi/a}^{(i)}$  (except for the highest excited band for which this is only approximately true).

### B. Strong coupling

In order to understand the physical background of the bands shown in Figs. 1 and 2, the strong-coupling and crossover regimes are examined separately in the following sections. In the strong-coupling regime the time scale relevant to the polaron translation is much slower than the time scale ( $1/\omega$ ) involved in the local polaron dynamics. Therefore, the local interplay between the electron density and the lattice deformation is almost independent of the polaron momentum. From the energy point of view the contributions corresponding to the polaron translation can be neglected, and the polarons can be treated, to a good approximation, as self-trapped. The deep potential well of the lattice deformation of the self-trapped polaron captures the electron. When the

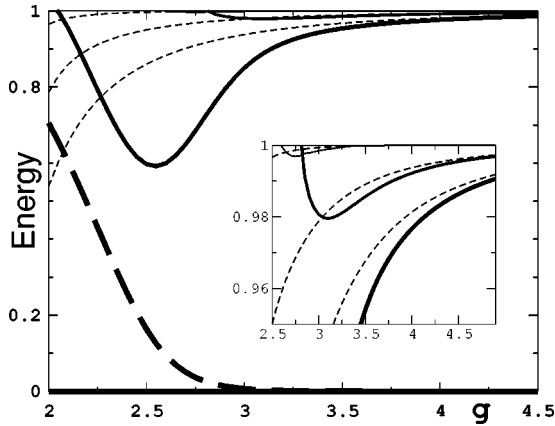


FIG. 3. The energies of  $K=0$  excited polaron states shifted by  $E_{K=0}^{(0)}$  (solid curves) are compared to the energies of the renormalized phonon excitations obtained by the strong-coupling adiabatic approximation of Ref. 5 (short-dashed curves). The long-dashed curve corresponds to  $E_{K=\pi/a}^{(0)}$  and shows the lowest band narrowing. The inset displays only a small part of the spectrum below  $E^{(c)} = 1$ .  $t = 2.5$  ( $\hbar\omega = 1$ ).

electron is light ( $\hbar\omega < t$ ), it is able to follow the slow motion of the lattice deformation (e.g., zero-point motion), which results in an adiabatic renormalization of the phonon modes within the lattice deformation.

The physical picture of the aforementioned self-trapped polaron follows from the adiabatic theory and can be considered to be well understood. Thus, in order to achieve a better understanding of the current numerical results, it is convenient to compare the renormalized phonon energies obtained in the adiabatic limit to the spectrum calculated by the ET method. For the Holstein polaron problem the renormalized phonon modes have been calculated by different adiabatic approximations.<sup>4-9,11</sup> The procedure of Ref. 5 (Born-Oppenheimer approximation therein Sec. III) treats the lattice discreteness directly, while the polaron translation is neglected. This approximation is appropriate for the present case as the lattice discreteness is important for the small self-trapped polarons, while the polaron translation has only a minor contribution to the energy.

The three short-dashed curves in Fig. 3 are the renormalized phonon energies of Ref. 5. The lowest excitation is a symmetric vibration of the lattice with respect to the polaron center (breathing mode). The next excitation is the antisymmetric vibration (pinning mode). The third excited mode is again a symmetric vibration, although extended over a larger number of lattice sites than in the case of the lowest excitation. In Fig. 3, the solid curves are the ET energies of the  $K=0$  polaron excited states. In the strong-coupling limit (the right part of Fig. 3) the results of Ref. 5 are recovered asymptotically, from below. The inset of Fig. 3, where only a small part of the spectrum below  $E^{(c)}$  is shown, clearly demonstrates this behavior. For strong couplings, the positions of the excited bands are given by the symmetric and antisymmetric phonon excitations of the adiabatic theory. In other words, the local dynamics of the self-trapped polarons is adiabatic.

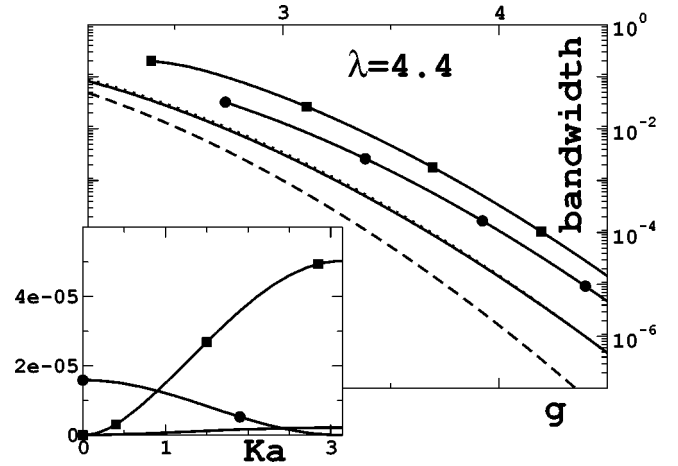


FIG. 4. The bandwidths (solid curves) of the three lowest polaron bands are plotted for  $2 \leq g \leq 5$  and  $\lambda = g^2/t \hbar\omega = 4.4$ . Each curve stops at the point where the top of the band crosses  $E^{(c)}$ . The bandwidths of the first and second excited bands are denoted by squares and circles, respectively. The long-dashed curve is the bandwidth of the nonadiabatic small polaron [ $\alpha = 1$  in Eq. (5)]. In the inset, the cosinelike ground and two excited bands of the self-trapped polaron are shown, shifted by  $E_{K=0}^{(i)}$ , as functions of momentum  $K$  ( $g=4$ ,  $t=5$ ,  $\lambda=3.2$ ). All the energies are in units of  $\hbar\omega$ .

The energy  $E_{K=\pi/a}^{(0)}$  is plotted as the long-dashed curve in Fig. 3. This curve defines the bandwidth of the lowest polaron band which can be seen to become large in the crossover regime (the left part of Fig. 3), as the translation of the polaron becomes important. On the other hand, in the strong-coupling limit, the ET method reproduces the narrow cosine polaron bands,

$$E_K^{(i)} - E_{K=0}^{(i)} \approx 2t_{pol}^{(i)} [1 - \cos(Ka)],$$

where  $t_{pol}^{(i)}$  is an effective polaron nearest-neighbor hopping energy for the  $i$ th excited state.

For strong couplings, the values of bandwidths may differ considerably from band to band. In Fig. 4 the bandwidths, as functions of  $g$ , are compared for constant  $\lambda = g^2/t \hbar\omega = 4.4$ . The solid curves are the results for the three lowest polaron bands. One sees that the effective hopping  $t_{pol}^{(i)}$  is increased if the polaron (i.e., the local lattice deformation) is excited. However, for strong couplings all bands are very narrow ( $4t_{pol}^{(i)} \ll \hbar\omega$ ), meaning that the polarons are very heavy (self-trapped). In real solids the coherent transport of such band states can be destroyed by the polaron-polaron interaction or by imperfections.<sup>36,37</sup>

A close inspection of the ET results in Fig. 4 reveals that the hopping energy  $t_{pol}^{(0)}$  of the self-trapped polaron for the lowest band is given by the simple relation

$$t_{pol}^{(0)} = t \exp[-(g/\hbar\omega)^2 \alpha(\lambda)]. \quad (5)$$

Equation (5) is an extension of the well-known expression for the nonadiabatic small-polaron hopping energy, which is obtained by setting  $\alpha = 1$ .<sup>10</sup>  $\alpha(\lambda)$  turns out to be a function of the adiabatic parameter  $\lambda$  only, i.e.,  $\alpha(\lambda)$  is an adiabatic

correction to the nonadiabatic small-polaron hopping. Notice that in the adiabatic limit  $\lambda$  defines the spreading of the lattice deformation (the polaron size  $\sim 1/\lambda$ ), as well as the renormalized phonon energies.<sup>5</sup> For  $\lambda = 4.4$  the excellent fit to the ET results in Fig. 4 (the short-dashed curve that follows almost exactly the ET results for the lowest band) is achieved with  $\alpha \approx 0.86$ , even though the bandwidth of the lowest polaron band changes by several orders of magnitude.

In summary, for the parameters under consideration (Fig. 4), it follows from Eq. (5) that the translational dynamics of the lowest band are essentially nonadiabatic, with adiabatic corrections. The narrow bandwidth defines the slow time scale for the polaron hopping. In contrast, Fig. 3 shows that the fast local dynamics of the self-trapped polarons is adiabatic. The adiabatic softening of the local phonon modes determines the positions of the ground and excited bands in the spectrum. The energy shift due to the softening is much larger than the bandwidths, which means that the polaron hopping can be neglected for the local dynamics.

### C. Crossover

In spite of the fact that the almost exact results for the lowest polaron band in the crossover regime, obtained by various numerical methods, have been known for quite some time, the corresponding qualitative explanation of the polaron properties does not appear completely satisfactory. It has been suggested in Ref. 38, by the use of the global-local method,<sup>39</sup> that a simple empirical relation between Hamiltonian parameters,

$$g_{ST} \approx \hbar \omega + \sqrt{t \hbar \omega}, \quad (6)$$

describes the regime for which the fast change from light to heavy polaron ground states takes place. Indeed,  $g_{ST}$  predicts, to a good approximation, the set of parameters for which the variation of the polaron effective mass (as a function of  $g$ ) is the fastest.

For  $t \gg \hbar \omega$  the crossover occurs in the adiabatic regime when  $g_{ST} \approx \sqrt{t \hbar \omega}$ —i.e.,  $\lambda_{ST} \approx 1$ . Approaching  $\lambda_{ST}$  from the strong-coupling adiabatic side ( $\lambda > \lambda_{ST}$ ), the size of the polaron increases. Consequently, the Peierls-Nabarro (PN) barrier decreases and tunneling of the adiabatic polaron to the neighboring sites becomes possible. This effect is also responsible for the coupling of the pinning and breathing lattice modes.<sup>40</sup> At  $\lambda < \lambda_{ST}$ , the restoring force of the pinning mode due to the PN barrier can be neglected, and one may treat the polaron as freely moving.<sup>7-9</sup> Such a scenario thus describes the crossover from the self-trapped (heavy) to propagating (light) polaron states in the adiabatic limit. On the other hand, for  $t \ll \hbar \omega$ , the nonadiabatic theory describes the polaron translation for arbitrary  $g$  and, in particular, at  $g = g_{ST} \approx \hbar \omega$  of Eq. (6). In this case, the polaron crossover appears essentially as a passage from the weak- to the strong-coupling ground state.

A reinspection of Fig. 2 shows that the two well-separated time scales found in the strong-coupling regime—one related to the polaron translation (given by the bandwidth) and the other related to the polaron local dynamics (given by the renormalized phonon energies)—become comparable in the

crossover regime. Furthermore, the behavior of the ground and excited bands for  $g \approx g_{ST}$  indicates that the polaron translation plays an important role in the excitation spectrum. In other words, the influence of the polaron hopping to the neighboring sites on the renormalized modes cannot be neglected under these conditions, as it can for strong couplings. The substantial difference in the crossover regime (see Fig. 3) between the ET results and the (adiabatically renormalized) phonon energies of Ref. 5 is explained in this way. This difference, however, is not necessarily related to nonadiabatic effects, as for the moderate values of the adiabatic ratio under current consideration ( $1 \lesssim t/\hbar \omega \lesssim 5$ ) it is not clear to what extent the nonadiabatic dynamics enters into the description of the polaron translation.

### D. Parity

Irrespective of their temporal (or spatial) properties, when the polaron bands cross and/or anticross as in Fig. 2, their symmetry properties become important. As already mentioned, the Holstein Hamiltonian is invariant under space inversion, and its eigenstates can be distinguished according to their parity. A simple linear transformation relates the momentum  $|\Psi_K^{(i)}\rangle$  and parity  $|\Psi_K^{(i)P}\rangle$  eigenstates,

$$|\Psi_K^{(i)P}\rangle = |\Psi_K^{(i)}\rangle \pm \hat{P} |\Psi_K^{(i)}\rangle = |\Psi_K^{(i)}\rangle \pm P |\Psi_{-K}^{(i)}\rangle,$$

so that

$$\hat{P} |\Psi_K^{(i)}\rangle = P |\Psi_{-K}^{(i)}\rangle. \quad (7)$$

$\hat{P}$  denotes the space inversion operator, and  $P = \pm 1$  are the even- and odd-parity eigenvalues, respectively.

Considering the ET method, the parity can be directly determined by inspection of the wave function properties. The eigenstates  $|\Psi_K^{(i)}\rangle$  can be expanded in terms of the basis states (4) with expansion coefficients  $a_{n_0, n_{-1}, n_1, \dots, n_m}$ :

$$|\Psi_K^{(i)}\rangle = \sum_{n_i} a_{n_0, n_{-1}, n_1, \dots, n_m} |n_0, n_{-1}, n_1, \dots, n_m\rangle_K.$$

$\hat{P}$  acting on the basis state (4) gives

$$\hat{P} |n_0, n_{-1}, n_1, \dots, n_m\rangle_K = |n_0, n_1, n_{-1}, \dots, n_m\rangle_{-K}.$$

Consequently, using Eq. (7) and the fact that  $|\Psi_{-K}^{(i)}\rangle$  is a complex conjugate of  $|\Psi_K^{(i)}\rangle$  (time reversal), one finds that the expansion coefficients satisfy

$$a_{n_0, n_{-1}, n_1, \dots, n_m} = P a_{n_0, n_1, n_{-1}, \dots, n_m}^*. \quad (8)$$

$a^*$  denotes the complex conjugate of  $a$ . The expansion coefficients in Eq. (8) stand for two local phonon configurations; the first one is obtained from the second one when the phonons to the left and right of the electron are interchanged ( $n_m \rightarrow n_{-m}$ ).

Applying the above analysis within the framework of the ET method yields  $P = -1$  for the second excited band ( $i = 2$ ), while  $P = 1$  for the ground and the other two lowest excited bands ( $i = 0, 1, 3$ ). In this respect, the polaron bands inherit the symmetry of the renormalized phonon modes as

obtained in the adiabatic limit. In Sec. IV B it was pointed out that the pinning mode corresponding to the second excited band is an antisymmetric vibration of the lattice (having odd parity), whereas the other two lowest excited modes are symmetric vibrations (having even parity). Furthermore, one sees that the crossing (rather than the anticrossing) between the excited bands in the crossover regime, shown in Fig. 2, involves bands of opposite symmetry under the space inversion.

For  $K=0$  and  $K=\pi/a$  the linear transformation<sup>19</sup> of the basis (4),

$$|n_0, n_{-1}, n_1, \dots, n_m\rangle_K^\pm = \frac{1}{\sqrt{2}} (|n_0, n_{-1}, n_1, \dots, n_m\rangle_K \pm |n_0, n_1, n_{-1}, \dots, n_{-m}\rangle_K), \quad (9)$$

defines two subspaces with different parities. It follows from Eq. (8) that the  $P=1$  eigenstates  $|\Psi_{K=0, \pi/a}^{(i)}\rangle$  belong to the + subspace of Eq. (9), while the  $P=-1$  eigenstates belong to the - subspace. One sees that for  $K=0$  and  $K=\pi/a$  the parity actually defines the symmetry of the local phonon configuration with respect to the electron. For  $P=1$  this configuration is symmetric, while it is antisymmetric for  $P=-1$ .

### E. Anticrossing

In Ref. 23 the correlated behavior of the ground and the first excited state in the crossover regime was analyzed for moderate values of the adiabatic ratio using a method based on the variational approach (see the CT method described in Sec. III B of Ref. 23). It was argued that the anticrossing of two physically different polaron states—one (heavy) for which the translation energy is almost negligible and the other (light) for which this energy is important—can describe in simple terms the mechanism of the crossover. It follows from this interpretation that by increasing  $g$  in the critical region of parameters near  $g_{ST}$  [Eq. (6)], the contribution to the ground state from the light state decreases in favor of the heavy state which has lower energy at stronger couplings. On the other hand, an opposite change occurs for the first excited state, which is heavier than the ground state for  $g \lesssim g_{ST}$ , while being lighter for  $g \gtrsim g_{ST}$ .

In Fig. 5 the polaron ground and first excited energies obtained in Ref. 23, denoted by CT, are compared to those of the ET method. Although the CT energies may be considered as a fair approximation, the anticrossing picture can be discussed more accurately in the context of the current ET results. One sees that the ET results confirm that the minimum of  $E_{K=0}^{(1)} - E_{K=0}^{(0)}$ , the two states of the same symmetry ( $P=1$ ), corresponds to  $g \approx g_{ST}$ . It is important to notice that the  $P=-1$  states of the second excited band ( $i=2$ ) (Fig. 2) are not involved in the anticrossing. The rest of the investigation presented here is focused on the polaron effective mass and on the properties of the lattice deformation.

The polaron effective mass  $m_{eff}^{(i)}$  can be evaluated numerically by using the relation<sup>18,22</sup>

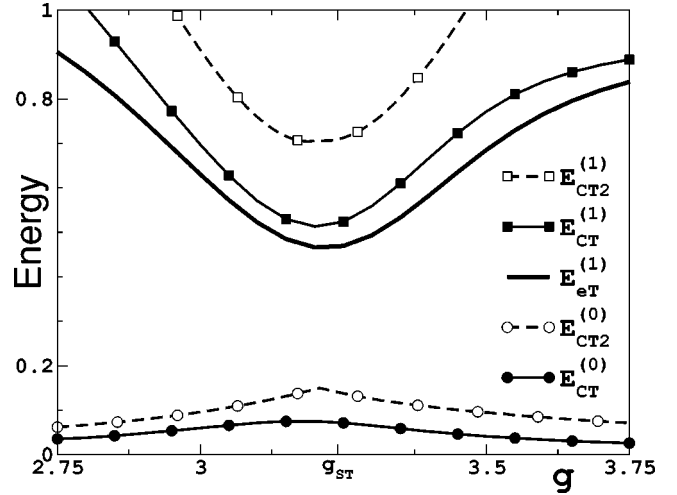


FIG. 5. The ground- and first excited-state energies obtained by the CT method of Ref. 23 and the first excited-state energy obtained by the ET method plotted as functions of  $g$ . The chosen set of parameters is the same as for Fig. 3 of Ref. 23,  $t=5$ ,  $g_{ST} \approx 3.24$  ( $\hbar\omega=1$ ),  $K=0$ . All curves are shifted by the ground-state ET energy.

$$m_{el}/m_{eff}^{(i)} = \frac{1}{t} \frac{E_{K=\Delta k}^{(i)} - E_{K=0}^{(i)}}{(\Delta ka)^2}, \quad (10)$$

where  $\Delta k$  is a small finite deviation of the momentum from the value  $K=0$ .  $m_{el}$  is the effective mass of the electron, and  $i$  denotes the band number. The ground- ( $m_{eff}^{(0)}$ ) and the first excited- ( $m_{eff}^{(1)}$ ) state effective masses are compared for  $t=1$  in Fig. 6. Although  $m_{eff}^{(0)} > m_{eff}^{(1)}$  for  $g \gtrsim g_{ST}$ ,  $m_{eff}^{(1)}$  becomes smaller than  $m_{eff}^{(0)}$  as  $g$  decreases. For larger  $t$ , the results are qualitatively the same (e.g., see Fig. 9), which means that the anticrossing picture indeed matches the behavior of  $m_{eff}^{(0)}$  and  $m_{eff}^{(1)}$  near  $g_{ST}$ .

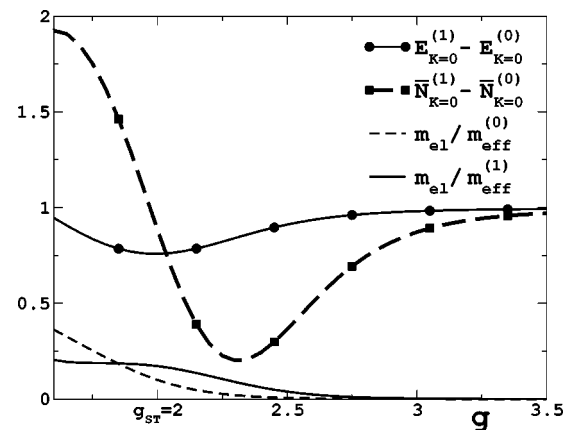


FIG. 6. Difference of the energy, the mean number of phonons (11), and the effective mass (10) of the ground and first excited states for  $t=1$  ( $\hbar\omega=1$ ). The minima of  $E_{K=0}^{(1)} - E_{K=0}^{(0)}$  and  $\bar{N}_{K=0}^{(1)} - \bar{N}_{K=0}^{(0)} = \bar{N}_{K=0}^{(0)} + 1$  almost coincide with  $g_{ST}=2$ . Notice that for  $g \lesssim g_{ST}$  the lowest excited state becomes heavier than the ground state ( $m_{eff}^{(1)} > m_{eff}^{(0)}$ ).

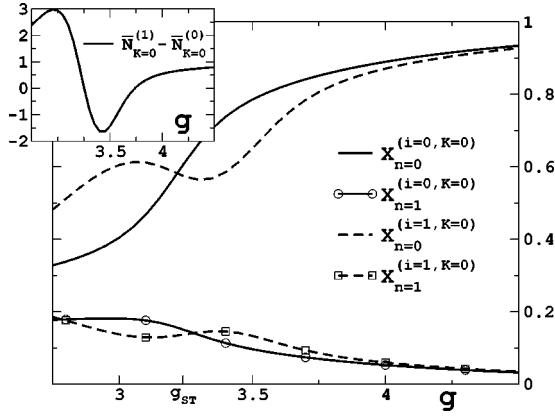


FIG. 7. The electron-lattice deformation correlation function  $X_n^{(i,K)}$ , Eq. (13), plotted as a function of  $g$  for  $n=0$  and  $n=1$ . In the former case  $X_n^{(i,K)}$  gives the correlation at the electron site, while in the latter it gives the correlation between the electron and lattice deformation at the neighboring site. The difference between the mean number of phonons in the ground and first excited states is shown in the inset.  $t=5$ ,  $K=0$ ,  $g_{ST} \approx 3.24$  ( $\hbar\omega=1$ ).

For fixed  $g$ , the mean total lattice deformation (3) is the same for the ground and excited states. However, the local phonon cloud around the electron can be more or less localized, which affects the polaron hopping to the neighboring sites. A light state implies that the associated local lattice deformation is spread to a larger number of lattice sites than for the heavy state. Namely, such a deformation gives rise to a greater effective hopping integral.

The mean number of phonons in the polaron state is given by

$$\bar{N}_K^{(i)} = \langle \Psi_K^{(i)} | \sum_m b_m^\dagger b_m | \Psi_K^{(i)} \rangle. \quad (11)$$

In the adiabatic limit, this number is quadratic in the local lattice deformation for the ground state. A more localized (heavier) lattice deformation leads to larger  $\bar{N}_K^{(0)}$ . Within the adiabatic approximation the excited renormalized phonon should, in general, increase the mean number of phonons with respect to  $\bar{N}_K^{(0)}$ . Particularly, in the strong-coupling limit one obtains

$$\lim_{g \rightarrow \infty} \bar{N}_K^{(1)} = \bar{N}_K^{(0)} + 1, \quad (12)$$

as the renormalization of the lattice vibrations becomes negligible.

From Fig. 6, in which  $\bar{N}_K^{(1)} - \bar{N}_K^{(0)}$  is plotted as a function of  $g$ , one sees that the ET results tend to Eq. (12) for strong couplings. In the crossover regime, on the other hand,  $\bar{N}_K^{(1)} - \bar{N}_K^{(0)}$  deviates from Eq. (12) considerably.  $\bar{N}_K^{(1)}$  is greater than  $\bar{N}_K^{(0)} + 1$  for  $g \leq g_{ST}$  and smaller than  $\bar{N}_K^{(0)} + 1$  for  $g \geq g_{ST}$ . For larger  $t$ , the amplitude of the deviation increases even further. As shown in the inset of Fig. 7,  $\bar{N}_K^{(1)} < \bar{N}_K^{(0)}$  for  $3.25 \leq g \leq 3.75$ , while the minimal and maximal values of  $\bar{N}_K^{(1)} - \bar{N}_K^{(0)}$  define an interval of almost five phonons.

Additional insights into the local polaron properties can be provided by studying the appropriate electron-lattice correlation function

$$X_n^{(i,K)} = \frac{\hbar\omega}{2g} \langle \Psi_K^{(i)} | \sum_m c_m^\dagger c_m (b_{m+n}^\dagger + b_{m+n}) | \Psi_K^{(i)} \rangle. \quad (13)$$

$X_n^{(i,K)}$  is the mean lattice deformation induced at the  $n$ th site away from the electron. The correlation function (13) is normalized in such a way that  $\sum_n X_n^{(i,K)} = 1$ . As the correlation spreads to adjacent lattice sites, the correlation at the electron site  $X_0^{(i,K)}$  decreases. Consequently,  $X_0^{(i,K)}$  should be larger for the heavy than for the light polaron state.

The ground- and first excited-state results for  $X_n^{(i,K=0)}$  are plotted in Fig. 7. The relationship between  $X_0^{(0,0)}$  and  $X_0^{(1,0)}$  changes near  $g_{ST}$ . This is exactly what one would expect from the anticrossing picture.  $X_0^{(0,0)} < X_0^{(1,0)}$  for  $g \leq g_{ST}$ . As the contribution of the heavy state to the ground state becomes dominant for  $g \geq g_{ST}$ , the relationship changes, and  $X_0^{(0,0)} > X_0^{(1,0)}$ . The spreading of the lattice deformation as a function of  $g$  may also be deduced from  $X_1^{(0,0)}$  and  $X_1^{(1,0)}$ . The results corresponding to this lattice site, shown in Fig. 7, again lead one to the same conclusion. For  $g \leq g_{ST}$  the lattice deformation seems to spread more for the ground than for the excited state and vice versa for  $g \geq g_{ST}$ .

All of the aforementioned ground- and first excited-state properties (the energy, the effective mass, the mean number of phonons, and the electron-lattice deformation correlation function) indicate that for  $t/\hbar\omega \lesssim 5$  the anticrossing of two (light and heavy) polaron states occurs near  $g_{ST}$ . Although criteria such as  $E_{K=0}^{(1)} - E_{K=0}^{(0)}$  being minimal,  $m_{eff}^{(1)} = m_{eff}^{(0)}$ ,  $X_0^{(0,0)} = X_0^{(1,0)}$ , or alternative criteria, do not agree exactly, they all predict the polaron crossover to occur within the same very narrow parameter range, given approximately by Eq. (6).

## V. ELECTRON PROPERTIES

### A. Single-electron spectral function

Denoting the vacuum state by  $|0\rangle$ , the zero-temperature single-electron Green function can be expressed as<sup>41,42</sup>

$$G_K(E) = \langle 0 | c_K \frac{1}{E - \hat{H} + i0^+} c_K^\dagger | 0 \rangle.$$

For the energies below the phonon threshold  $E < E^{(c)}$  no polaron-phonon scattering takes place, which has the consequence that the imaginary part of the electron self-energy  $\Sigma_K(E < E^{(c)})$  tends to zero.<sup>12,13</sup> Accordingly, the low-energy part of the spectral function  $A_K(E)$ , denoted by  $A_K^<(E)$ , is defined by the simple poles of  $G_K(E)$  at  $E = E_K^{(i)}$ :

$$A_K^<(E < E^{(c)}) = \sum_i |\langle \Psi_K^{(i)} | c_K^\dagger \rangle|^2 \delta(E - E_K^{(i)}); \quad (14)$$

i.e., the spectral function  $A_K^<(E)$  is defined by the polaron energy  $E_K^{(i)}$  and the quasiparticle weight  $Z_K^{(i)} = |\langle \Psi_K^{(i)} | c_K^\dagger \rangle|^2$ .



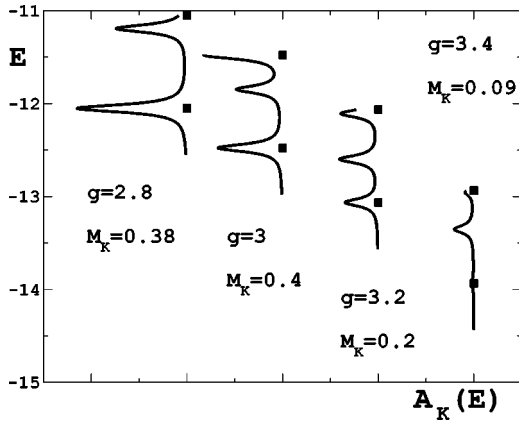


FIG. 8.  $A_K^<(E)$  given by Eq. (14) is plotted for  $t=5$ ,  $K=0$ , and four values of  $g$  in the crossover regime. All spectra are broadened by a Lorentzian of width 0.05. For each curve the lower square denotes  $E=E_{K=0}^{(0)}$ , while the higher one denotes  $E=E^{(c)}$ . Notice that for  $g \geq g_{ST} \approx 3.24$ , the spectral weight associated with the first excited state is larger than the one associated with the ground state.  $M_K$ , given by Eq. (15), is the total normalized spectral weight of the ground and excited polaron states (below the phonon threshold).

In particular, for  $K=0$  and  $K=\pi/a$ , the quasiparticle weight  $Z_{K=0,\pi/a}^{(i)}$  vanishes by parity for the  $P=-1$  eigenstates  $|\Psi_{K=0,\pi/a}^{(i)}\rangle$ , because the free-electron (zero-phonon) state  $|c_{K=0,\pi/a}^\dagger\rangle$  belongs to the  $+$  subspace of Eq. (9).

In Fig. 8,  $A_{K=0}^<(E)$  is plotted as a function of  $E$  for a few different values of  $g$  in the crossover regime. The spectral weight corresponding to the ground polaron state is of the same order of magnitude as the one corresponding to the excited (even-parity) polaron states. Moreover,  $M_K$  defined by

$$M_K = \int A_K^<(E) dE, \quad (15)$$

reveals that, in the crossover regime (for  $g \leq g_{ST}$ ), nearly 40% of the total spectral weight confined to the ground and excited polaron states can be located in the energy window below the phonon threshold. Therefore, at least for  $g \sim g_{ST}$  and for the values of adiabatic ratio under current considerations ( $t/\hbar\omega \leq 5$ ), the results imply the existence of a few well-pronounced peaks in the single-electron spectral density below the phonon threshold. For stronger couplings, on the other hand, the quasiparticle weight below the phonon threshold is almost completely suppressed.

### B. Electron self-energy

When the electron propagator  $G_K(E)$  is expressed in terms of the electron self-energy  $\Sigma_K(E)$ , both  $Z_K^{(i)}$  and  $E_K^{(i)}$  of Eq. (14) can be related to  $\Sigma_K(E)$ . E.g., the polaron effective mass  $m_{eff}^{(i)}$  is given in terms of the self-energy  $\Sigma_K(E)$  by the standard formula<sup>43</sup>

$$m_{el}/m_{eff}^{(i)} = \frac{1 + \partial_{\varepsilon_K} \Sigma_K(E)}{1 - \partial_E \Sigma_K(E)} = Z_{K=0}^{(i)} (1 + \gamma^{(i)}), \quad (16)$$

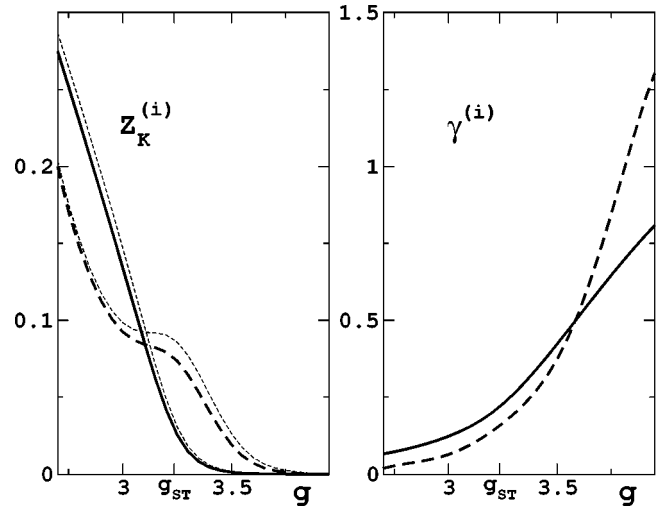


FIG. 9.  $Z_{K=0}^{(i)}$  and  $\gamma^{(i)}$  given by Eq. (16) are plotted in the left and right panels, respectively ( $t=5$ ,  $g_{ST} \approx 3.24$ ,  $\hbar\omega=1$ ). The solid curves are the ground-state results; the long-dashed curves are the first excited-state results. In the left panel the short-dashed curves show the inverse effective mass  $m_{el}/m_{eff}^{(i)}$ .

where  $1/Z_K^{(i)} = 1 - \partial_E \Sigma_K(E)$  and  $\varepsilon_K = K^2 a^2 t = \hbar^2 K^2 / 2m_{el}$ . In Eq. (16),  $i$  is used to distinguish between results for the ground and excited (even-parity) states.  $\gamma^{(i)}$  is the abbreviation for the appropriately normalized  $K$ -dependent contribution to  $m_{eff}^{(i)}$ .

When the self-energy  $\Sigma_K(E)$  is local ( $K$  independent,  $\gamma^{(i)}=0$ ) the polaron effective mass is related solely to the quasiparticle weight  $Z_{K=0}^{(i)}$ . Thus, the nonlocal character of the self-energy can be investigated by comparing  $\gamma^{(i)}$  to unity.<sup>24</sup> Such an analysis is particularly interesting in the context of DMFT, as the locality (implying  $\gamma^{(i)}=0$ ) of the self-energy is an essential ingredient of this approach.<sup>13</sup> In both the weak-coupling ( $g \rightarrow 0$ ) and nonadiabatic ( $t \rightarrow 0$ ) limits,  $\Sigma_K(E)$  becomes local.<sup>13,18,41</sup> Within the Holstein-Lang-Firsov approximation<sup>10,41</sup> and for  $t \rightarrow 0$ , the self-energy  $\Sigma_K(E) = \Sigma(E)$  is, to a good approximation, given by its expansion to the first order in  $E$  over the whole energy range defined by the lowest band. In this case,  $Z_K^{(0)} \approx Z^{(0)}$  defines the renormalization of the narrow cosinelike lowest band for any  $K$ .

With the ET method  $\gamma^{(i)}$  can be obtained in terms of  $Z_{K=0}^{(i)}$  and  $m_{eff}^{(i)}$ , the latter being estimated numerically from the band dispersion at the center of the Brillouin zone [Eq. (10)]. The ET results agree with the aforementioned analytical findings for small  $t$  and/or  $g$  (Ref. 24). It follows that significant nonlocal contributions to  $\Sigma_K(E)$  can possibly occur in the regime where neither  $t$  nor  $g$  are small. In the left panel of Fig. 9,  $Z_{K=0}^{(i)}$  is plotted for moderate  $t$  as function of  $g$ , while the right panel shows  $\gamma^{(i)}$  for the same set of parameters. Although  $\gamma^{(i)}$  does not contribute to  $m_{eff}^{(i)}$  substantially for  $g \leq g_{ST}$ , at stronger couplings  $\gamma^{(i)}$  reaches values of the order of unity for both the ground and first excited states. That is, the nonlocal contribution to the electron self-energy is as equally important as the local one. However, it should be noticed that, in this regime, the quasiparticle weight  $Z_K^{(i)}$  becomes small.

### C. Optical conductivity

The interband optical conductivity may be evaluated within the linear-response theory from the current-current correlation function. The low-energy (coherent) contribution to the real part of the interband conductivity at zero temperature is given by<sup>16,44</sup>

$$\sigma_R^<(E) = \sum_{i \neq 0} \frac{|\langle \Psi^{(i)} | \hat{J} | \Psi^{(0)} \rangle|^2}{E^{(i)} - E^{(0)}} \delta(E - E^{(i)} + E^{(0)}), \quad (17)$$

where  $|\Psi^{(i)}\rangle$  are the  $K=0$  polaron states, herein calculated by the ET method. The incoherent contribution to the interband conductivity, denoted by  $\sigma_R^>(E)$ , corresponds to the continuum of the excitation spectrum above the phonon threshold. Since the current operator in Eq. (17), defined by

$$\hat{J} = it \sum_n (c_{n+1}^\dagger c_n - c_n^\dagger c_{n+1}),$$

is odd under space inversion, the nonvanishing matrix elements in Eq. (17) are those between the  $P=1$  ground state  $|\Psi^{(0)}\rangle$  and  $P=-1$  excited states  $|\Psi^{(i)}\rangle$ . Actually, the incoherent part of the interband optical conductivity  $\sigma_R^>(E)$  involves only  $P=-1$  excitations as well. On the contrary, as argued in Eq. (14), the spectral function  $A_K(E)$  contains information about the  $P=1$  part of the spectrum at  $K \approx 0$ . The optical conductivity at zero temperature is therefore described by those excited states for which the quasiparticle weight  $Z_{K \approx 0}$  vanishes—i.e., those states that are not seen in the single-electron spectral function.

The real part of the optical conductivity  $\sigma_R(E)$  includes the interband part and the (intraband) Drude term at  $E \approx 0$ . It follows from the well-known sum rule<sup>44</sup> that the total spectral weight of  $\sigma_R(E)$  is given by the mean value of the electron kinetic energy in the ground state. Consequently, not only is the ET method capable of calculating  $\sigma_R^<(E)$ , but the total spectral weight of  $\sigma_R(E)$  is also accessible. Furthermore, one may estimate the weight of the Drude term from the polaron effective mass.<sup>20</sup>

According to the ET results, for  $t \leq 5$  there is only one interband transition  $|\Psi_{K=0}^{(0)+}\rangle \rightarrow |\Psi_{K=0}^{(2)-}\rangle$  which contributes at zero temperature to  $\sigma_R^<(E)$  [Eq. (17)]. It is interesting to find the corresponding non-Drude spectral weight below the phonon threshold. However,  $E_{K=0}^{(2)}$  is less than  $E^{(c)}$  for relatively strong couplings, for which most of the spectral weight of  $\sigma_R(E)$  belongs to high energies. In this parameter regime only a few percent (or less) of the total spectral weight of  $\sigma_R(E)$  corresponds to  $\sigma_R^<(E)$  or to the Drude term. This simple low-energy picture of  $\sigma_R(E)$  becomes certainly more complex at finite temperature, particularly in the crossover regime where the bandwidths of the coherent polaron states increase. Studies at finite temperature, however, require different methods than the one presented here.

### VI. SUMMARY

This paper reports an exact-diagonalization study of the ground and excited polaron states in the one-dimensional Holstein model. For values of the adiabatic ratio  $t/\hbar\omega \leq 5$ , accurate energies and wave functions are obtained for translationally invariant solutions of the infinite lattice problem. The chosen method is restricted to the part of the spectrum below the phonon threshold, for which there are no phonon excitations uncorrelated to the polaron.

The eigenstates of the Holstein Hamiltonian can be distinguished according to their parity. This property follows from the Hamiltonian which is invariant under space inversion. It is shown that only the odd excited states of the system are relevant to the optical conductivity at zero temperature. However, the contribution of the coherent excited polaron state is rather small with respect to the total spectral weight. On the other hand, it is the even states that contribute to the single-electron spectral function for  $K \approx 0$ . In this case, the contribution of the coherent excited polaron states is found to be important, particularly in the crossover regime.

In the strong-coupling regime the results agree with the picture of self-trapped polarons, which may be regarded as well understood. The spectrum is characterized by very small polaron bandwidths. Consequently, the time scale associated with the polaron translation is very large, and the contributions to the fast local polaron dynamics from the polaron hopping are negligible. By making a comparison with the ET results, it is shown that the adiabatic theory (the Born-Oppenheimer approximation) provides a good description of the local properties of the self-trapped polaron. Namely, the energies of the renormalized phonon excitations are close to the ET excited-band energies. Two of the excited bands correspond to the symmetric adiabatic vibrations of the lattice, while one corresponds to the antisymmetric (pinning) vibration. Finally, it is found that for strong couplings the electron self-energy shows significant nonlocal ( $K$ -dependent) behavior at moderate  $t$ .

As the electron-phonon coupling decreases at moderate  $t$ , the simple band structure found in the strong-coupling regime (i.e., the narrow and well-separated polaron bands) evolves notably. The effective hopping integral of the ground and excited polaron states defines a time scale which, in the crossover regime, is comparable to the time scale relevant for the local polaron dynamics. In the crossover regime the excited (odd-parity) band, which corresponds to the pinning vibration in the strong-coupling regime, crosses the other two (even-parity) bands, which correspond to symmetric vibrations. The results suggest that the same critical set of parameters defined by  $g_{ST}$  [Eq. (6)], found for the polaron ground-state crossover, may also be associated with the rapid change of the low-energy excitation spectrum.

Aside from the fact that the polaron translation and the local dynamics mix in the crossover regime, the intermediate (moderate) values of the adiabatic ratio employed herein present additional difficulties for qualitative understanding. Namely, for  $1 \leq t/\hbar\omega \leq 5$ , both the adiabatic and nonadiabatic contributions could be important for the polaron crossover. Nevertheless, in the context of the ET approach, analy-

ses of the energy, the effective mass, and the lattice deformation properties all agree in one important respect. That is, for moderate values of the adiabatic ratio, two polaron states of even parity (one heavy and one light) undergo an anticrossing in the same region of parameters for which the ground state crosses over from the weak- to the strong-coupling regime.

## ACKNOWLEDGMENT

This work was supported in part by Project No. SCOPES-7KPJ065619 of the Swiss National Science Foundation. The calculations were performed mainly on the PC cluster system of the Institute of Physics in Zagreb, donated by the Alexander von Humboldt Foundation.

\*Electronic address: obarisc@ifs.hr

- <sup>1</sup>L.D. Landau, Phys. Z. Sowjetunion **3**, 644 (1933).
- <sup>2</sup>S.I. Pekar, J. Phys. (Moscow) **10**, 341 (1946).
- <sup>3</sup>T. Holstein, Ann. Phys. (N.Y.) **8**, 325 (1959).
- <sup>4</sup>V.V. Kabanov and O.Yu. Mashtakov, Phys. Rev. B **47**, 6060 (1993).
- <sup>5</sup>G. Kalosakas, S. Aubry, and G.P. Tsironis, Phys. Rev. B **58**, 3094 (1998).
- <sup>6</sup>N.K. Voulgarakis and G.P. Tsironis, Phys. Rev. B **63**, 014302 (2000).
- <sup>7</sup>V.I. Mel'nikov, Sov. Phys. JETP **45**, 1233 (1977).
- <sup>8</sup>P.B. Shaw and G. Whitfield, Phys. Rev. B **17**, 1495 (1978).
- <sup>9</sup>T.D. Holstein and L.A. Turkevich, Phys. Rev. B **38**, 1901 (1988); A.H. Castro Neto and A.O. Caldeira, *ibid.* **46**, 8858 (1992).
- <sup>10</sup>T. Holstein, Ann. Phys. (N.Y.) **8**, 343 (1959).
- <sup>11</sup>A.S. Alexandrov, V.V. Kabanov, and D.K. Ray, Phys. Rev. B **49**, 9915 (1994).
- <sup>12</sup>S. Engelsberg and J.R. Schrieffer, Phys. Rev. **131**, 993 (1963).
- <sup>13</sup>S. Ciuchi, F. de Pasquale, and D. Feinberg, Europhys. Lett. **30**, 151 (1995); S. Ciuchi, F. de Pasquale, S. Fratini, and D. Feinberg, Phys. Rev. B **56**, 4494 (1997).
- <sup>14</sup>J. Ranninger and U. Thibblin, Phys. Rev. B **45**, 7730 (1992); E.V.L. de Mello and J. Ranninger, *ibid.* **55**, 14 872 (1997).
- <sup>15</sup>M. Capone, W. Stephan, and M. Grilli, Phys. Rev. B **56**, 4484 (1997).
- <sup>16</sup>C. Zhang, E. Jeckelmann, and S.R. White, Phys. Rev. B **60**, 14 092 (1999).
- <sup>17</sup>G. Wellein and H. Fehske, Phys. Rev. B **58**, 6208 (1998).
- <sup>18</sup>H. Fehske, J. Loos, and G. Wellein, Phys. Rev. B **61**, 8016 (2000).
- <sup>19</sup>M. Hoffmann and Z.G. Soos, Phys. Rev. B **66**, 024305 (2002).
- <sup>20</sup>S. El Shawish, J. Bonča, L.-C. Ku, and S.A. Trugman, Phys. Rev. B **67**, 014301 (2003).
- <sup>21</sup>S. Fratini, F. de Pasquale, and S. Ciuchi, Phys. Rev. B **63**, 153101 (2001).
- <sup>22</sup>J. Bonča, S.A. Trugman, and I. Batistić, Phys. Rev. B **60**, 1633 (1999).
- <sup>23</sup>O.S. Barišić, Phys. Rev. B **65**, 144301 (2002).
- <sup>24</sup>L.-C. Ku, S.A. Trugman, and J. Bonča, Phys. Rev. B **65**, 174306 (2002).
- <sup>25</sup>G. Wellein and H. Fehske, Phys. Rev. B **56**, 4513 (1997).
- <sup>26</sup>L. Proville and S. Aubry, Eur. Phys. J. B **15**, 405 (2000).
- <sup>27</sup>N.V. Prokof'ev and B.V. Svistunov, Phys. Rev. Lett. **81**, 2514 (1998); A.S. Mishchenko, N.V. Prokof'ev, A. Sakamoto, and B.V. Svistunov, Phys. Rev. B **62**, 6317 (2000).
- <sup>28</sup>S.I. Pekar, E.I. Rashba, and V.I. Sheka, Zh. Eksp. Teor. Fiz. **76**, 251 (1979).
- <sup>29</sup>A.S. Mishchenko *et al.*, Phys. Rev. B **66**, 020301(R) (2002).
- <sup>30</sup>D. Feinberg, S. Ciuchi, and F. de Pasquale, Int. J. Mod. Phys. B **4**, 1395 (1990).
- <sup>31</sup>J.M. Robin, Phys. Rev. B **56**, 13 634 (1997).
- <sup>32</sup>J. K. Cullum and R. A. Willoughby, *Lanczos Algorithms for Large Symmetric Eigenvalue Computations* (Birkhäuser, Boston, 1985).
- <sup>33</sup>G. H. Golub and C. F. van Loan, *Matrix Computations* (The Johns Hopkins University Press, Baltimore, 1989).
- <sup>34</sup>H. Haken, Z. Phys. **139**, 56 (1954); G. Whitfield and R. Puff, Phys. Rev. **139**, A338 (1965).
- <sup>35</sup>Y. Zhao, D.W. Brown, and K. Lindenberg, J. Chem. Phys. **107**, 3159 (1997); J.M. Robin, Phys. Rev. B **58**, 14 335 (1998).
- <sup>36</sup>A.S. Alexandrov, Phys. Rev. B **61**, 12 315 (2000).
- <sup>37</sup>E.V.L. de Mello and J. Ranninger, Phys. Rev. B **58**, 9098 (1998).
- <sup>38</sup>A.H. Romero, D.W. Brown, and K. Lindenberg, Phys. Rev. B **59**, 13 728 (1999).
- <sup>39</sup>D.W. Brown, K. Lindenberg, and Y. Zhao, J. Chem. Phys. **107**, 3179 (1997).
- <sup>40</sup>O. S. Barišić (unpublished).
- <sup>41</sup>A.S. Alexandrov and J. Ranninger, Phys. Rev. B **45**, 13 109 (1992).
- <sup>42</sup>P.E. Kornilovitch, Europhys. Lett. **59**, 735 (2002).
- <sup>43</sup>G. D. Mahan, *Many-Particle Physics* (Plenum Press, New York, 1990).
- <sup>44</sup>P.F. Maldague, Phys. Rev. B **16**, 2437 (1977); E. Dagotto, Rev. Mod. Phys. **66**, 763 (1994).